Photoselection and the Appearance of Franck−Condon-Forbidden Thresholds in the ZEKE Spectrum of NO_2

Hiroshi Matsui, Jane M. Behm, and Edward R. Grant*

Department of Chemistry, Purdue University, West Lafayette, Indiana 47907

Received: February 13, 1997; In Final Form: April 4, 1997[⊗]

Photoionizing transitions that change NO_2^+−core vibrational quantum numbers are examined by means of zero-kinetic-energy (ZEKE) threshold photoelectron spectroscopy. Observable intensity is found in Franck−Condon-off-diagonal transitions from the (000) vibrational ground state of the 3pσ $^2\Sigma_u^+$ Rydberg state of NO_2 to long-lived resonances at thresholds corresponding to (010), (02^00), and (100) vibrationally excited states of NO_2^+. Analyses of the rovibrational structure of the originating Rydberg state and the cation establish that NO_2^+−core potential energy surfaces are in each case substantially parallel and thus predict zero Franck−Condon factors for transitions that change vibrational quantum numbers. The appearance of nonvertical transitions is attributed to the mixing of long-lived high-principal-quantum-number discrete Rydberg states that converge to each excited threshold with the optically accessible ground-state free-electron continuum. The vibrationally inelastic interaction that gives rise to this Franck−Condon-forbidden threshold structure mirrors the common one in which discrete Rydberg states converging to a vibrationally excited threshold decay by vibrational autoionization to an underlying relaxed-core continuum. In the present case, continuum states reached in vertical excitation form long-lived resonances by borrowing lifetime from discrete high-*n* states converging to vibrationally excited thresholds. Apparently, the discrete character conveyed in each case is sufficient to permit evolution in the Stark manifold that stabilizes ZEKE states for detection by pulsed-field ionization. This is the first example of a continuum stabilized by the ZEKE Stark-mixing mechanism. The extent of the effect observed at each threshold is consistent with patterns of electron−core coupling strengths established by mode-dependent trends in vibrational autoionization linewidths.

I. Introduction

Photoselection is an important tool in the contemporary study of chemical dynamics. Stepwise excitation strategies have been widely used to prepare molecules for state-to-state fragmentation,[1−7] and intermediate-state mediation has provided a well-demonstrated means to control the course of chemical transformations.[8,9] Work in our laboratory has shown that vibrational autoionization in polyatomic molecules, which can be viewed as a kind of fragmentation, exhibits dynamics that are quite sensitive to the normal mode selected for vibrational relaxation.[10] In NO_2, where bend-stretch Fermi resonance couples higher vibrationally excited states, we find that mode specificity diminishes with increasing level of vibrational excitation.[11] The apparent decrease in vibrational mode control in this case serves to illustrate some of the limitations that mode mixing or intramolecular redistribution (IVR) can impose on control strategies that rely on photoselection.

Photoselection strategies have played an important role in zero-kinetic-energy (ZEKE) high-resolution threshold photoelectron spectroscopy,[12] where stepwise excitation isolates individual transitions to reduce rovibrational congestion and provide information on state-to-state photoionization cross sections.[13] Interestingly, however, ZEKE detection also depends for its existence on state-mixing; relatively short-lived Rydberg states which are optically accessible must evolve to develop anomalously long lifetimes.[14,15] Originally, there was some question whether the source of this lifetime lengthening was best assigned to redistribution in the manifold of cation−core excited rovibrational states[16] or in the orbital density of states accessible to the Rydberg electron in an electrostatic field.[14,15,17−19] Numerous studies have shown evidence of Rydberg−Rydberg coupling involving transfer of energy and angular momentum between Rydberg-orbital and core-rovibrational degrees of freedom,[20−28] but most workers now agree that the dominant mechanism for lifetime lengthening lies in the field-induced evolution of the Rydberg electronic degree of freedom in the nonpenetrating space of high l and m_l.[29−32]

In earlier work, we used three-color rovibrational selection to study the ZEKE spectrum of NO_2 in strong vertical 3pσ Rydberg-to-threshold transitions.[33] Our results characterized the rotational and vibrational structure of the cation, including a moderate bend−stretch Fermi resonance,[34] which is present to virtually the same degree in the cation core of the originating 3pσ Rydberg state.[35] Our ZEKE spectra also show evidence for significant final-state Rydberg−Rydberg rotational coupling, which confers the long lifetimes of rotationally forbidden thresholds on interloping low-*n* Rydberg states to which transitions are rotationally allowed.[24] High-*n* Rydberg states converging to all vibrationally excited thresholds are subject to prompt decay by vibrational autoionization. From linewidths in vibrational autoionization spectra, we know that coupling strengths are strongly mode dependent, favoring symmetric stretch over bend and asymmetric stretch, and we find that ZEKE intensities, reflecting the loss of population, are weaker for vertical transitions to excited symmetric stretching thresholds than those associated with bending and asymmetric stretching modes.[25]

The present work establishes that all of the same vibrationally excited thresholds observed in vertical transitions from vibrationally excited levels of the 3pσ Rydberg state can be seen in transitions from the 3pσ origin. Because the vibrational force fields of the 3pσ Rydberg state and the cation are virtually identical, one might expect these transitions to be excluded by zero Franck−Condon factors. We argue that the source of the

[⊗] Abstract published in *Advance ACS Abstracts,* August 1, 1997.

S1089-5639(97)00556-2 CCC: $14.00

Franck−Condon-forbidden intensity exhibited here is the same discrete−continuum autoionization interaction that diminishes intensities in the vertical ZEKE spectrum of vibrationally excited thresholds and parallels the discrete−discrete and continuum−discrete−discrete mechanisms that produce transitions in the Franck−Condon gap well-known in VUV−ZEKE and conventional threshold photoelectron spectroscopy.[36,37]

In sections below we offer an explanation for the present observations in which we suggest that the oscillator strength for Franck−Condon-forbidden vibrationally excited thresholds is carried by Franck−Condon-allowed transitions to the energetic-electron continuum of the cation ground state. In regions isoenergetic with vibrationally excited thresholds, continuum states populated by excitation from 3pσ (000) are stabilized by the autoionization coupling of this bright continuum with high-n Rydberg states subject to field-induced stabilization. Based on this interpretation, we submit that the signal observed in these experiments constitutes the first example of a continuum stabilized by the ZEKE Stark-mixing mechanism. In accord with the extent of mixing expected on the basis of the coupling hierarchy observed in vibrational autoionization, we find that the survival fraction (ZEKE intensity) reverses the trend seen in vertical excitation: Stabilization by lifetime borrowing from discrete near-threshold Rydberg states favors cores excited in symmetric stretch and states mixed with symmetric stretch by core vibrational coupling.

II. Experiment

We use standard methods of ZEKE photoelectron spectroscopy.[12,13,21,25] The sample gas, NO_2, seeded 1:1:20 in O_2/He is cooled by expansion through a differentially pumped pulsed-jet source (General Valve, IOTA 1). The skimmed molecular beam enters a magnetically shielded longitudinally oriented ZEKE spectrometer through the first plate (repeller) of a three-gridded-plate ion-optics assembly. Three superimposed laser beams cross the molecular beam between the repeller and second (extractor) plates, which are spaced by about 2.5 cm. The distance between the beam valve and the point of excitation is about 7.5 cm. For the present experiments, intermediate rotational levels of the 3pσ $^2\Sigma_u^+$ (000) Rydberg state are selected by double resonance. The third laser then promotes the excited molecules to successive ionization thresholds and scans the rovibronic structure of the (000), (010), (020), and (100) thresholds of NO_2^+. The near-threshold high-Rydberg electrons are freed by delayed field ionization (from 2 to 5 μs delay) and detected by a two-plate multichannel electron detector. The extractor is held near ground and a pulse of from −800 mV to −2.4 V is applied to the repeller as required to obtain a detectable ZEKE signal. The ZEKE signal is amplified and collected by a LeCroy 9450 digital oscilloscope.

Tunable radiation for the first and second excitation steps is provided by Lambda Physik 3002 and 2002 dye lasers pumped by a single EMG 201 MSC XeCl excimer laser. A single-mode Optical Parametric Oscillator (OPO, Continuum Mirage 500) pumped by a seeded Continuum Powerlite 8000 Nd:Yag laser is used for the third step. The bandwidths of the dye lasers are 0.2 cm^{-1}, and that of the OPO is 0.01 cm^{-1}. The wavelengths of the lasers are calibrated using a Burleigh W-4500 pulsed wavemeter.

III. Results

A. State Selection at the 3pσ $^2\Sigma_u^+$ (000) Rydberg State. As shown in the schematic energy level diagram in Figure 1, we achieve rotational and vibrational selection at the 3pσ $^2\Sigma_u^+$ (000) Rydberg state in two sequential steps of resonant excitation. The first laser, tuned in the visible region to 20 857 cm^{-1}, promotes ground-state NO_2 to its mixed $^2B_1$, $^2B_2$, $^2A_2$ system of long-lived, low-lying excited electronic states. After a delay of approximately 20 ns, a second laser elevates excited molecules to the 3pσ $^2\Sigma_u^+$ (000) Rydberg state, using an ultraviolet photon energy at 34 748 cm^{-1}. A third laser, which promotes transitions to the (000), (010), (020), and (100) ionization thresholds, is delayed 15 ns and tuned through energies between 21 600 and 23 100 cm^{-1}. By fixing the energies of the second and the third photons on a specific transition and scanning the first laser, we can obtain a spectrum of the rotational levels of the ground state from which the three-color process originates.

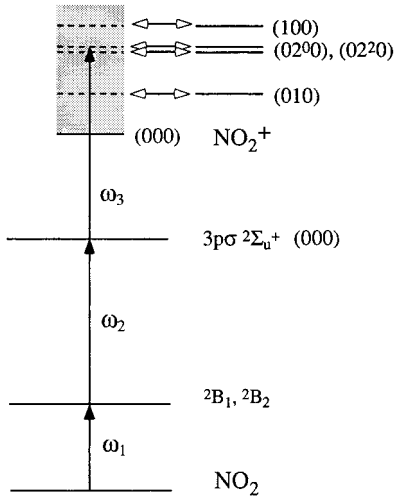

Figure 1. Energy level diagram showing the triple resonance scheme used to excite NO_2 from its ground state through the 3pσ (000) Rydberg state to various photoionization thresholds. Arrows illustrate discrete−continuum interactions.

For all vibronic states of $N^{16}O_2$, nuclear-spin statistics allow only states symmetric in the exchange of the nuclei. Thus, all vibrational states have permutation-inversion symmetry either (+,S) or (−,S).[38] This symmetry is determined by the electronic symmetry of the σ_u Rydberg electron combined with the rovibronic symmetry of the cation core. For the cation ground state, the vibronic symmetry of the core is Σ_g. For states that are vibronically Σ, nuclear-spin statistics exclude certain rotational quantum numbers. Thus, only odd rotational quantum numbers, N', are present for the 3pσ (000) vibronic state.

Upon selecting a first-photon transition that originates from the specific ground state rotational level, $N'' = 1$, we tune the second laser to reach the $N' = 3$ rotational level of the 3pσ $^2\Sigma_u^+$ (000) Rydberg state. Two-photon selection rules allow transitions strictly from − to −, or from + to +. This has the effect of constraining the ground-state prolate-top K substates from which transitions to various Rydberg vibrational levels can originate. Thus, two-photon selection rules allow transitions to (000) only from $K'' =$ odd, and all our jet-cooled spectra originate from $K'' = 1$.

B. Rotational Assignments for the (000), (010), (020), and (100) States of the Cation. Figures 2−4 show threshold photoionization spectra resolving vertical transitions to (000) and non-Franck−Condon transitions to (010), (020), and (100) vibrational states of the cation. Each of these spectra originate from the $N' = 3$ rotational level of the 3pσ $^2\Sigma_u^+$ (000) Rydberg state. The energies shown are referenced to the $K'' = 0$, $N'' = 0$ ground state. All spectra are recorded using identical electron extraction fields. Surveying signal levels in succession under constant instrumental conditions, we find peak intensities for

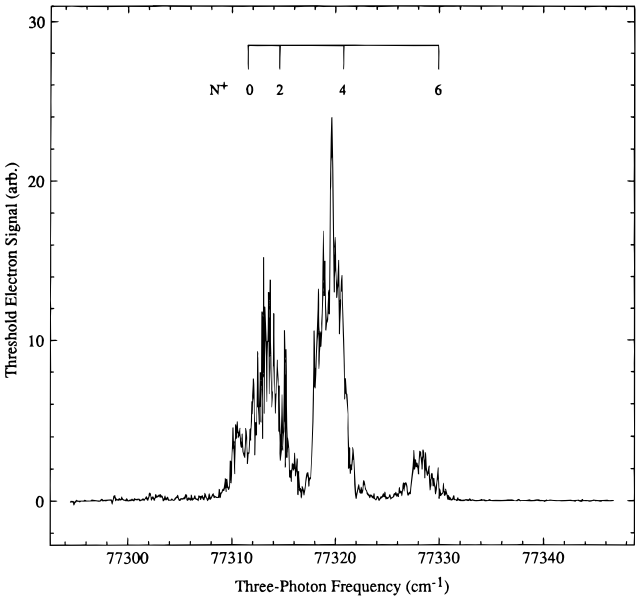

Figure 2. ZEKE high-resolution threshold photoionization spectrum of NO_2^+ (000) observed in transitions from the 3pσ (000) $N' = 3$ intermediate Rydberg state. Frequencies are referenced to the neutral ground-state $N'' = 0$, $K'' = 0$ level.

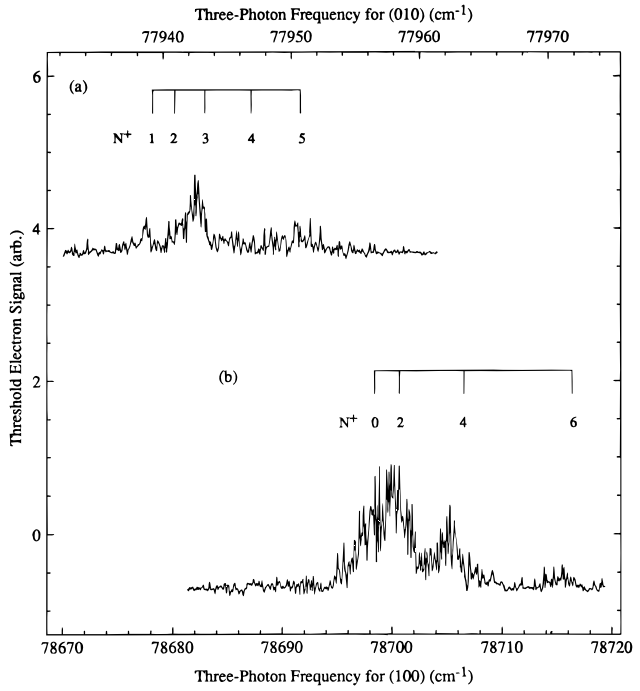

Figure 3. (a) ZEKE high-resolution threshold photoionization spectrum of NO_2^+ (010) observed in transitions from 3pσ (000) $N' = 3$. (b) ZEKE threshold spectrum of NO_2^+ (100) observed in transitions from 3pσ (000) $N' = 3$. Frequencies are referenced to the neutral ground-state $N'' = 0$, $K'' = 0$ level. Ladders mark the positions of rotational levels determined by vertical scans.

transitions from 3pσ (000) $N' = 3$ to cation thresholds (000), (100), (02^00), and (010) to fall in the ratio 15:3:2:1, respectively.

Totally symmetric thresholds such as (000), (02^00), and (100) exhibit structure assigned to the cationic rotational levels $N^+ = 0, 2, 4, 6$. Structure at the (010) threshold, which, for the isolated cation, has Π_u vibronic symmetry, is assigned as $N^+ = 1, 2, 3, 4, 5$. The spectrum at the Δ_g (02^20) threshold displays transitions to $N^+ = 2, 3, 4, 5$. Although this transition is very weak, such assignment is suggested upon comparison with the vertical threshold spectrum from the 3pσ (02^20) intermediate state to cationic (02^20). The relative energies of the ionization

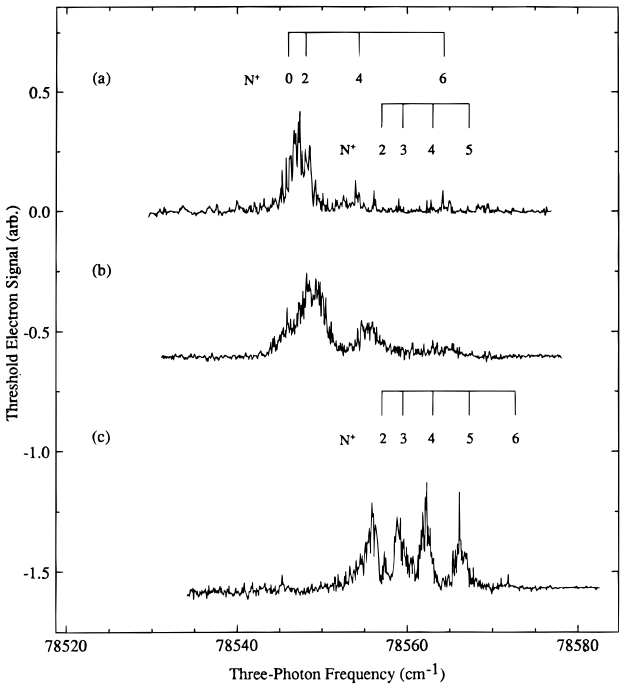

Figure 4. ZEKE high-resolution threshold photoionization spectrum of NO_2^+ (020) (a) observed in transitions from 3pσ (000) $N' = 3$ (off-diagonal transition), (b) observed in transitions from 3pσ (02^00) $N' = 3$ (vertical transition), and (c) observed in transitions from 3pσ (02^20) $N' = 3$ (vertical transition). All frequencies are referenced to the neutral ground-state $N'' = 0$, $K'' = 0$ level. Ladders mark the positions of rotational levels determined by vertical scans.

TABLE 1: Relative Vibrational and Rotational Positions in the ZEKE Spectra of NO_2[a]

		vibrational state				
species	rot state N^+	(000)	(010)	(02^00)	(02^20)	(100)
NO_2^+	0	0		1234.4		1386.8
	1		627.7			
	2	3.0	1.6	2.0	1245.2	2.3
	3		4.1		2.5	
	4	9.2	7.4	8.2	5.9	8.2
	5		11.7		10.2	
	6	18.4	16.8	17.8		17.8
NO_2 3pσ	0	0		1238.0		1401.1
	1		621.2			
	2				1250.7	

[a] Band origins except (02^20) are established by reference to transitions from the same intermediate Rydberg state, 3pσ (000) $N' = 3$. The positions of individual rotational states within vibrationally excited bands are determined by stronger perpendicular scans from corresponding levels of vibrational excitation in the 3pσ Rydberg state. The lowest rotational energy for each excited vibrational state of the cation is given in relation to the threshold energy for producing the (000), $N^+ = 0$ state of the cation. Higher rotational energies are given with respect to corresponding band origins. All values are in cm^{-1}.

thresholds for various rotational and vibrational states with respect to the (000) $N^+ = 0$ state of the ion are listed in Table 1.

IV. Discussion

A. Transitions from the 3pσ $^2\Sigma_u^+$ (000) Rydberg State to Photoionization Thresholds at (010), (020), and (100) States of NO_2^+. The vibrational frequencies of the NO_2^+ cation match those of the neutral 3pσ Rydberg state to within a few wavenumbers. This correspondence suggests that the potential energy surfaces for the Rydberg core and the free cation are substantially parallel (at least in the harmonic region). Under

such conditions, vibrational wave functions in the two systems should be well-described by the same set of orthonormal wave functions, which leads one to expect that Frank-Condon factors will strongly favor transitions from 3pσ ($v_1v_2v_3$) to the same set of vibrational quantum numbers ($v_1v_2v_3$) in the cation. In the data, however, we see substantial intensity in non-Franck−Condon transitions from zero-point 3pσ (000) to high-n Rydberg states converging to vibrationally excited thresholds, including (100), (010), (02^00), and (02^20).

Earlier work in our laboratory has used strong vertical transitions from selected 3pσ Rydberg levels to populate high-n (ZEKE) Rydberg states converging to like vibrational levels of NO_2^+.[24,25,33,34] Such scans, of which Figure 2 is representative, resolve individual rotational lines. In zeroth order, the intensities of these lines can be expected to conform with a simple picture based on angular momentum selection rules for Hund's case b to case d transitions.[25] In particular, for initial $l = 1$ to final $l = 0$ and 2, angular-momentum conservation constrains ΔN to $-3 \leq (N^+ - N') \leq 3$. In the data, we find that the upper limit on final rotational quantum number uniformly fits with this constraint, but negative ΔN rotational branches show transitions to forbidden low-N^+ thresholds. Similar low-N^+ intensity anomalies have been seen in other systems.[21−23]

Detailed examination of these spectra in the case of NO_2 shows resolved reproducible substructure within the ZEKE-detection bandwidth about each forbidden threshold. Comparing this substructure with the complete photoionization spectrum shows that these features coincide with rotationally autoionizing lower-n Rydberg series converging to angular-momentum-accessible higher rotational thresholds. The presence of this structure as a long-lived component of the delayed pulsed-field (ZEKE) photoionization spectrum suggests that the structure due to nominally forbidden thresholds arises by discrete−discrete coupling of bright but intrinsically short-lived low-n/high-N^+ Rydberg states with the dense manifold of long-lived high-n Rydberg states associated with isoenergetic forbidden low-N^+ thresholds.

Transitions to low-n/high-N^+ Rydberg states are of course allowed everywhere. The autoionization of these states gives rise to the complex prompt-electron autoionization spectrum. However, at energies coinciding with lower-N^+ thresholds, these allowed states can borrow lifetime by rotational coupling with high-n Rydbergs. The high-n Rydberg character thereby derived is apparently sufficient to allow these mixed Rydberg states to begin evolving in the l, m_l Stark manifold to form long-lived ZEKE states that survive for detection by pulsed-field ionization.

The transfer of intensity from accessible autoionizing states to nominally forbidden thresholds is well-known in conventional threshold photoelectron spectroscopy as a mechanism for transferring intensity to the Franck−Condon gap in diatomic and triatomic molecules.[36] In VUV ZEKE experiments, such discrete−discrete coupling effects populate vibrational levels as high as $v^+ = 25$ in H_2 and O_2.[37] In essence, this same mechanism can be called upon to explain the presence of non-Franck−Condon features in the ZEKE spectrum of NO_2.

In the scans presented above, we find unexpected transitions from the 3pσ (000) ground state to excited vibrational thresholds that are nominally forbidden by zero Franck−Condon factors. However, throughout this range of the spectrum, perpendicular transitions are fully allowed from 3pσ (000) to the continuum of the cation vibrational ground state. This continuum is coupled to discrete high-Rydberg states converging to vibrationally excited thresholds by the same interactions that give rise to vibrational autoionization. At all third-photon wavelengths, excitation produces prompt electrons by direct photoionization. But in addition, at total excitation energies coincident with those of the excited thresholds, autoionization interactions mix the bright continuum with high-n discrete Rydbergs.

As a result of their high-Rydberg character, discrete−continuum mixed states in the narrow regions about Franck−Condon-forbidden thresholds apparently possess sufficient lifetime to begin evolution in l and m_l space induced by the electrostatic fields of the apparatus and adventitious ions. This evolution provides the lifetime lengthening necessary for detection by delayed pulsed ionization. The probability of stabilization of such mixed configurations accessed by transitions from the 3pσ (000) ground state should be little different from that of vibrationally excited (and autoionizing) high-Rydbergs reached at the same thresholds in vertical transitions from 3pσ ($v_1v_2v_3$) excited states.

That high-resolution PFI-ZEKE threshold discrimination relies on the lifetime lengthening, which occurs when optically accessible, low-l, high-n Rydberg states evolve in applied electrostatic fields to form high-l, high-m_l ZEKE states, is well-recognized.[17−19,29−32] The present results show that this stabilization can be achieved even when the threshold to which the high-Rydberg states converge is Franck−Condon forbidden and oscillator strength comes from transitions to the underlying *continuum*. The fraction of excited molecules at a given threshold that survive to begin evolving in the Stark manifold depends on the extent of discrete character in the mixture. This in turn depends on the strength of the vibrational autoionization interaction that couples the high-n Rydbergs at that particular threshold with the (000) continuum.

We know from direct studies of lower-n autoionizing Rydberg series that this interaction is nonzero for all of the vibrationally excited states of interest here. But it also varies significantly from state to state. Vibrational autoionization linewidths show that symmetric stretch, and bending overtones mixed by Fermi resonance with symmetric stretch, couple more effectively than bend. This differentiation must arise in the close-range Rydberg-electron−core interaction that precedes evolution to high $l-m_l$ states. Such a separation, in which a close-coupled core interaction affects the properties of long-range Coulomb states, is a central feature of multichannel quantum defect theory, and thus MQDT provides a natural framework in which to consider the effects of discrete−continuum vibrational coupling on ZEKE intensities.

B. ZEKE Intensities and the Dynamics of Vibrational Autoionization. Multichannel quantum defect theory explicitly treats the scattering interactions that occur when Rydberg electrons in penetrating orbitals collide with the core and transfer energy and angular momentum between orbital electronic and molecular vibrational and rotational degrees of freedom.[39−42] Close to the core, where coupling occurs, the fast-moving electron samples a single internuclear separation, undergoing interactions that are largely independent of its asymptotic energy. The appropriate basis in this collision-channel region consists of the Born−Oppenheimer products of electronic functions, i, with core vibrational wavefunctions, written $|iR\Lambda\rangle^{JM}$, where i represents a generalized electronic quantum number, R is the internuclear distance, and Λ is the well-defined projection of the total orbital angular momentum on the internuclear axis.

Close-coupled scattering states are mixed by the R-dependent electronic $\mathbf{K}^\Lambda(R)$ matrix, which follows directly from the electronic or eigenchannel quantum defect matrix, $\mu^\Lambda(R)$. A rovibrational frame transformation projects collision-channel interactions on the manifold of asymptotic states to define the full rovibronic $\mathbf{K}$ matrix. The elements of this matrix,

$K_{iv_i^+N_i^+,jv_j^+N_j^+}$, define long-range channel wave functions corresponding to scattering states, $\Psi_{iv_i^+N_i^+}{}^{JM}(E)$, in which, at total energy E, an electron with energy $\epsilon_{iv_i^+N_i^+}$ and angular momentum l_i collides with a cation in electronic-vibrational−rotational state $|iv_i^+\ N_i^+\rangle^{JM}$ to produce a final state that is a mixture of all accessible channels, $|\epsilon_{jv_j^+N_j^+}\rangle|jv_j^+N_j^+\rangle^{JM}$. Thus,

$$\Psi_{iv_i^+N_i^+}{}^{JM}(E) = f_i(r,\epsilon_{iv_i^+N_i^+})|iv_i^+N_i^+\rangle^{JM} + \sum_{jv_j^+N_j^+} K_{iv_i^+N_i^+jv_j^+N_j^+} \times g_j(r,\epsilon_{jv_j^+N_j^+})|jv_j^+N_j^+\rangle^{JM}$$

where f_i $(r,\epsilon_{iv_i^+N_i^+})$ and $g_j(r,\epsilon_{jv_j^+N_j^+})$ denote the energy-dependent basis of regular and irregular Coulomb wave functions, and the full **K** matrix is constructed from the R-dependent short-range interaction by[39−41]

$$K_{iv_i^+N_i^+,jv_j^+N_j^+} = \int \mathrm{d}R\, {}^{JM}\langle iv_i^+N_i^+|\{\sum_{\Lambda}|iR\Lambda\rangle^{JM}K_{ij}{}^{\Lambda}(R)^{JM}\langle jR\Lambda|\}|jv_j^+N_j^+\rangle^{JM}$$

in which,

$$K_{ij}{}^{\Lambda}(R) = \tan \pi\, \mu_{ij}{}^{\Lambda}(R)$$

The long-range channel wave functions formed by these short-range interactions comprise the states that are mixed with purely nonpenetrating high-l Coulomb wave functions by instrumental electrostatic fields to form long-lived ZEKE states.

For a triatomic molecule, R spans the full space of the normal coordinates. The magnitude of the collision-channel integral over this space, and thus the size of the **K** matrix element that mixes vibrationally excited discrete Rydberg structure with the vertical continuum, depends on the coordinate dependence of the quantum defect matrix element, $\mu_{ij}{}^{\Lambda}(R)$. For diagonal elements, this dependence is given directly by the variation with R in the energy separation between the cation potential and that of the close-coupled Rydberg electronic state i. Off-diagonal elements of the quantum defect matrix reflect the vibronic coupling of different Rydberg electronic configurations. Magnitudes of these quantities determine adiabatic potential energy surface geometries in the neighborhood of diabatic crossings.

For present purposes we confine our attention to the coordinates for symmetric stretch and bend (R_1 and R_2). At geometries for which $R_2 \neq 0$, the quantum defect matrix factors as shown in Table 2. Diagonal elements yield symmetric collision-channel terms that leave l unchanged. These give rise to **K** matrix elements that link the totally symmetric (000) continuum with even $l = 0$ and 2 discrete Rydberg states converging to totally symmetric vibronically excited limits such as (100) and (02^00). Off-diagonal elements of the quantum defect matrix describe interactions that couple collision-channel states of different l. These interactions produce terms that mix the totally symmetric continuum with orbitally odd discrete states core-excited in asymmetric vibrational modes, such as $l = 1$ Rydberg states coverging to (010).

Angular momentum conservation determines rovibrational selection rules. These are simplest for totally symmetric states coupled by diagonal elements of the quantum defect matrix. Because they leave vibrational angular momentum unchanged, such interactions can conserve both N^+ and Rydberg electron orbital angular momentum. Coupling between the totally symmetric (000) continuum and high-n discrete states converging to the (010) bending excited state requires transfer of angular momentum between electronic and core vibrational and rotational degrees of freedom, the pattern of which varies according to whether the core-excited discrete states converge to even or odd N^+. Table 3 gives representative examples for zeroth-order continuum states with $l = 0$. The $l = 2$ continuum, also accessible from 3pσ (000), offers many more pathways for exchanging electronic, vibrational and rotational angular momentum.

Previous work in our laboratory has characterized this vibronic coupling from the point of view of autoionizing discrete states of lower principal quantum number reached in vertical transitions from 3pσ ($v_1v_2v_3$) excited states.[24,25,33,34] Linewidths in these spectra show that coupling to the continuum is strongly mode dependent, favoring symmetric stretch over bend and asymmetric stretch. This hierarchy extends to affect relative intensities observed in vertical ZEKE spectra, where, compared with other vibrationally excited states, spectra obtained at the (100) threshold are significantly weakened by the loss of near-threshold Rydberg states to vibrational autoionization. Coupling

TABLE 2: Quantum Defect Matrix for an ABA Triatomic Molecule Where $R = \{R_1,R_2,R_3\}$ and R_1 and R_2 (Symmetric Stretch and Bend) May Vary, But R_3 (Asymmetric Stretch) Is Constrained to Zero[a]

$D_{\infty h}$	Σ_g	Σ_g	Π_u	Π_g	Σ_u	Π_g	Π_u	
Σ_g	$\mu(R)_{ss}$	$\mu(R)_{sd}$	$\mu(R)_{sp}$					A_1
Σ_g	$\mu(R)_{sd}$	$\mu(R)_{dd}$	$\mu(R)_{dp}$					
Π_u	$\mu(R)_{sp}$	$\mu(R)_{dp}$	$\mu(R)_{pp}$					
Π_g				$\mu(R)_{dd}$	$\mu(R)_{dp}$			B_2
Σ_u				$\mu(R)_{dp}$	$\mu(R)_{pp}$			
Π_g						$\mu(R)_{dd}$		A_2
Π_u							$\mu(R)_{pp}$	B_1
	A_1			B_2		A_2	B_1	C_{2v}

[a] C_{2v} symmetry blocks show the off-diagonal elements that couple core vibrational states (000) and (010) by interactions between $l = 0$, 2 and $l = 1$. These matrix elements are zero for $R_2 = 0$ (linear geometry). See ref 42.

TABLE 3: Examples of Asymptotic Channel Functions Coupled by R-Dependent Short-Range Rydberg-Electron−Core Interactions in Which the Lifetime of High-n Rydberg States Converging to Excited Rovibrational Thresholds Is Conferred on the Ground-State Continuum; Following Excitation in Zeroth Order from 3pσ $^2\Sigma_u^+$ (000) to the $l = 0$ (s-Wave) Continuum for Various Rotational States of NO_2^+ $^1\Sigma_g^+$ (000)

cation plus free electron	high-n Rydberg states
(a) In the Energy Regions of the (100) Thresholds for Forming $N^+ = 0$, 2, 4, and 6	
$\|(000), l^+=0, N^+=0, N=0, \epsilon, l=0\rangle$	$\|(100), l^+=0, N^+=0, N=0, n, l=0\rangle$
$\|(000), l^+=0, N^+=2, N=2, \epsilon, l=0\rangle$	$\|(100), l^+=0, N^+=2, N=2, n, l=0\rangle$
$\|(000), l^+=0, N^+=4, N=4, \epsilon, l=0\rangle$	$\|(100), l^+=0, N^+=4, N=4, n, l=0\rangle$
$\|(000), l^+=0, N^+=6, N=6, \epsilon, l=0\rangle$	$\|(100), l^+=0, N^+=6, N=6, n, l=0\rangle$
(b) In the Energy Regions of the (010) Thresholds for Forming $N^+ = 1$, 2, 3, 4, and 5	
$\|(000), l^+=0, N^+=0, N=0, \epsilon, l=0\rangle$	$\|(010), l^+=1, N^+=1, N=0, n, l=1\rangle$
$\|(000), l^+=0, N^+=2, N=2, \epsilon, l=0\rangle$	$\|(010), l^+=1, N^+=1, N=2, n, l=1\rangle$
$\|(000), l^+=0, N^+=2, N=2, \epsilon, l=0\rangle$	$\|(010), l^+=1, N^+=2, N=2, n, l=1\rangle$
$\|(000), l^+=0, N^+=2, N=2, \epsilon, l=0\rangle$	$\|(010), l^+=1, N^+=3, N=2, n, l=1\rangle$
$\|(000), l^+=0, N^+=4, N=4, \epsilon, l=0\rangle$	$\|(010), l^+=1, N^+=3, N=4, n, l=1\rangle$
$\|(000), l^+=0, N^+=4, N=4, \epsilon, l=0\rangle$	$\|(010), l^+=1, N^+=4, N=4, n, l=1\rangle$
$\|(000), l^+=0, N^+=4, N=4, \epsilon, l=0\rangle$	$\|(010), l^+=1, N^+=5, N=4, n, l=1\rangle$
$\|(000), l^+=0, N^+=6, N=6, \epsilon, l=0\rangle$	$\|(010), l^+=1, N^+=5, N=6, n, l=1\rangle$

in that case adds continuum character to discrete thresholds accessible in vertical transitions. We argue above that the same vibrational autoionization interaction acts to produce vibrationally excited threshold structure in the nonvertical ZEKE spectrum from 3pσ (000). Note, however, that because in this case coupling confers discrete structure on an optically accessible continuum, stronger mixing raises the survival fraction and thus boosts ZEKE intensities. This expectation is in accord with our observations. Thresholds associated with vibrationally excited states (100) and (02^00), which lower-*n* linewidths show to be strongly autoionized, exhibit significantly higher non-Franck−Condon ZEKE intensities than more weakly interacting (010) and (02^20).

Acknowledgment. H.M. gratefully acknowledges a fellowship from the Purdue Research Foundation. E.R.G. thanks Christian Jungen and Stephen Pratt for helpful discussions. This work was sponsored by the U.S. Department of Energy under Grant No. DE-FG02-93ER14401.

References and Notes

(1) Jortner, J.; Levine, R. D. *Adv. Chem. Phys.* **1981**, *47* (1), 1.
(2) Crim, F. F. *Annu. Rev. Phys. Chem.* **1984**, *35*, 657.
(3) Schinke, R.; Engel, V.; Andresen, P.; Hausler, D.; Balint-Kurti, G. G. *Phys. Rev. Lett.* **1985**, *55*, 1180.
(4) Bigio, L.; Grant, E. R. *J. Phys. Chem.* **1985**, *89*, 5855. Bigio, L.; Grant, E. R. *J. Chem. Phys.* **1987**, *87*, 360.
(5) *Mode Selective Chemistry*, Jortner, J., Levine, R. D., Pullman, B., Eds.; Kluwer: Dordrecht, 1991.
(6) Schinke, R. *Photodissociation Dynamics*; Cambridge University Press: Cambridge, 1993.
(7) Lester, M. I. *Adv. Chem. Phys.* **1996**, *96*, 51.
(8) Crim, F. F. *Annu. Rev. Phys. Chem.* **1993**, *44*, 397.
(9) Bronikowski, M. J.; Simpson, W. R.; Zare, R. N. *J. Phys. Chem.* **1993**, *97*, 2194, 2204.
(10) Campos, F. X.; Jiang, Y.; Grant, E. R. *J. Chem. Phys.* **1990**, *93*, 2308, 7731; **1991**, *94*, 5897. Bryant, G.; Jiang, Y.; Grant, E. R. *J. Chem. Phys.* **1992**, *96*, 4827.
(11) Matsui, H.; Grant, E. R. *J. Chem. Phys.* **1996**, *104*, 42.
(12) Müller-Dethlefs, K.; Schlag, E. W. *Annu. Rev. Phys. Chem.* **1991**, *42*, 109. Schlag, E. W.; Müller-Dethlefs, K.; Wang, K.; McKoy, V.; Grant, E. R. *Adv. Chem. Phys.* **1995**, *90*, 1.
(13) de Lange, C. A. In *High Resolution Laser Photoionization and Photoelectron Studies*; Powis, I., Baer, T., Ng, C. Y., Eds.; John Wiley and Sons Ltd.: New York, 1995; p 195.
(14) Chupka, W. A. *J. Chem. Phys.* **1993**, *98*, 4520.
(15) Merkt, F.; Zare, R. N. *J. Chem. Phys.* **1994**, *101*, 3495.
(16) Even, U.; Ben-Nun, M.; Levine, R. D. *Chem. Phys. Lett.* **1993**, *210*, 416. Scherzer, W. G.; Selzle, H. L.; Schlag, E. W.; Levine, R. D. *Phys. Rev. Lett.* **1994**, *72*, 1435. Rabani, E.; Levine, R. D.; Even, U. *J. Phys. Chem.* **1994**, *98*, 8834.
(17) Merkt, F.; Fielding, H. H.; Softley, T. P. *Chem. Phys. Lett.* **1993**, *202*, 153.
(18) Jortner, J.; Bixon, M. *J. Chem. Phys.* **1995**, *102*, 5636. Bixon, M.; Jortner, J. *J. Phys. Chem.* **1995**, *99*, 7466.
(19) Vrakking, M. J. J.; Lee, Y. T. *J. Chem. Phys.* **1995**, *102*, 8818, 8833.
(20) Gilbert, R. D.; Child, M. S. *Chem. Phys. Lett.* **1991**, *187*.
(21) Wiedmann, R. T.; Grant, E. R.; Tonkyn, R. G.; White, M. G. *J. Chem. Phys.* **1991**, *95*, 746. Tonkyn, R. G.; Wiedmann, R.; Grant, E. R.; White, M. G. *J. Chem. Phys.* **1991**, *95*, 7033. Tonkyn, R. G.; Wiedmann, R. T.; White, M. G. *J. Chem. Phys.* **1992**, *96*, 3696. Lee, M.-T.; Wang, K.; McKoy, V.; Tonkyn, R. G.; Wiedmann, R. T.; Grant, E. R.; White, M. G. *J. Chem. Phys.* **1992**, *96*, 7848.
(22) Grant, E. R.; White, M. G. *Nature*, **1991**, *354*, 249.
(23) Merkt, F.; Softley, T. P. *J. Chem.Phys.* **1992**, *96*, 4149. Merkt, F.; Mackenzie, S. R.; Softley, T. P. *J. Chem.Phys.* **1995**, *103*, 4509.
(24) Bryant, G.; Jiang, Y.; Martin, M.; Grant, E. R. *J. Phys. Chem* **96**, 6875 (1992).
(25) Bryant, G. P.; Jiang, Y.; Martin, M.; Grant, E. R. *J. Chem. Phys.* **1994**, *101*, 7199.
(26) Vrakking, M. J. J. *J. Chem. Phys.* **1996**, *105*, 7336.
(27) Remacle, F.; Levine, R. D. *J. Chem. Phys.* **1996**, *105*, 4649.
(28) Bixon, M.; Jortner, J. *Mol. Phys.* **1996**, *89*, 373.
(29) Ramacle, F.; Levine, R. D. *J. Chem. Phys.* **1996**, *104*, 1399. Rabani, E.; Levine, R. D. *J. Chem. Phys.* **1996**, *104*, 1937. Remacle, F.; Levine, R. D.; Schlag, E. W.; Selzle, H. L.; Held, A. *J. Phys. Chem.* **1996**, *100*, 15320. Remacle, F.; Even, U.; Levine, R. D. *J. Phys. Chem.* **1996**, *100*, 19735.
(30) Bixon, M.; Jortner, J. *J. Phys. Chem.* **1996**, *100*, 11914.
(31) Merkt, F.; Rednall, R. J.; Mackenzie, S. R.; Softley, T. P. *Phys. Rev. Lett.* **1996**, *76*, 3526.
(32) Dietrich, H.-J.; Müller-Dethlefs, K.; Ya.Baranov, L. *Phys. Rev. Lett.* **1996**, *76*, 3531.
(33) Bryant, G.; Jiang, Y.; Grant, E. R. *Chem. Phys. Lett.* **1992**, *200*, 495.
(34) Matsui, H.; Behm, J. M.; Grant, E. R. *Int. J. Mass Spectrom. Ion Processes*, in press.
(35) Matsui, H.; Mayer, E. E.; Grant, E. R. *J. Mol. Spectrosc.* **1996**, *175*, 203.
(36) Guyon, P. M.; Baer, T.; Nenner, I. *J. Chem. Phys.* **1983**, *78*, 3665. Baer, T.; Guyon, P. M. *J. Chem. Phys.* **1986**, *85*, 4765. Chupka, W. A.; Miller, P. J.; Eyler, E. E. *J. Chem. Phys.* **1988**, *88*, 3032. Guyon, P. M.; Gislason, E. A. *Topics in Current Chemistry*; Springer-Verlag: Berlin, 1989; Vol. 151, pp 161−178.
(37) Kong, W.; Rodgers, D.; Hepburn, J. W. *Chem. Phys. Lett.* **1993**, *203*, 497. Kong, W.; Hepburn, J. W. *Can. J. Phys.* **1994**, *72*, 1284. Martin, J. D. D.; Alcaraz, C.; Mank, A.; Kong, W.; Hepburn, J. W. *Proc. SPIE* **1995**, *2548*, 74.
(38) Mulliken, R. S. *Phys. Rev.* **1941**, *59*, 873 (1941).
(39) See for example: Greene, C.; Jungen, Ch. *Adv. At. Mol. Phys.* **1985**, *21*, 51. Ross, S. C. *AIP Conf. Proc. 225*, 73.
(40) Raoult, M.; Jungen, Ch. *J. Chem. Phys.* **1981**, *74*, 3388.
(41) Ross, S. C.; Jungen, Ch. *Phys. Rev. A* **1994**, *49*, 4353, 4364; **1994**, *50*, 4618.
(42) Jungen, Ch.; Pratt, S. T. *J. Chem. Phys.* **1997**, *106*, 9529.